Spectrochimica Acta Part A: Molecular and Biomolecular Spectroscopy 188 (2018) 64–71

Contents lists available at ScienceDirect

Spectrochimica Acta Part A: Molecular and Biomolecular Spectroscopy

journal homepage: www.elsevier.com/locate/saa

Φ-order spectrophotokinetic characterisation and quantification of *trans-cis* oxyresveratrol reactivity, photodegradation and actinometry

Mounir Maafi *, Mohammed Ahmed Al-Qarni

Leicester School of Pharmacy, De Montfort University, The Gateway, Leicester LE1 9BH, UK

ARTICLE INFO

Article history:
Received 1 March 2017
Received in revised form 13 June 2017
Accepted 30 June 2017
Available online 02 July 2017

Keywords:
Oxyresveratrol
Photodegradation
Φ-order kinetic
Quantum yield
Actinometry

ABSTRACT

A new Φ-order kinetic method was proposed in this study for the investigation of *trans-cis* photoisomerization reaction of Oxyresveratrol (ORVT) subjected to non-isosbestic irradiation. In ethanolic media, it has been proven that forward ($\Phi^{\lambda_{irr}}_{A\rightarrow B}$) and reverse ($\Phi^{\lambda_{irr}}_{B\rightarrow A}$) reaction quantum yields were dependent on the monochromatic irradiation wavelength according to sigmoid patterns over the spectral ranges of their electronic absorption (260–360 nm). An 11.4- and 6.6-fold increases were recorded for $\Phi^{\lambda_{irr}}_{B\rightarrow A}$ and $\Phi^{\lambda_{irr}}_{A\rightarrow B}$, respectively. The efficiencies of the former ($\Phi^{\lambda_{irr}}_{B\rightarrow A}$, ranging between 2.3×10^{-2} and 26.3×10^{-2}) were 33 to 60% smaller than those of the respective $\Phi^{\lambda_{irr}}_{A\rightarrow B}$ measured at the irradiation wavelengths selected. Overall, between 57 and 97% degradation of the initial *trans*-ORVT was observed under relatively weak light intensities, with the highest values recorded at the longest wavelengths. These findings strongly recommend protection from light in all situations of this biologically important phytomolecule that possesses therapeutic value of interest to pharmaceutical applications. The Φ-order kinetics also offered a simple way to develop a reliable actinometric method that proved ORVT to be an efficient actinometer for the dynamic range 295–360 nm. The usefulness of Φ-order kinetics for the investigation and quantification of phytoproducts' photodegradation was discussed.

1. Introduction

Oxyresveratrol (ORVT) belongs to the stilbenoid group of phytomolecules that is widely found in plants and fruits such as peanuts, raspberries, blueberries, tea, and highly concentrated in grapes and wine [1]. The anti-oxidative properties have long been known for hydroxystilbenoids [2] as well as for ORVT [3]. The latter molecule has been attributed a number of other biological effects including but not limited to being antiviral [4], hepatoprotective [5], anti-tumor [6,7] and anti-herpes [8]. In addition, ORVT has neuroprotective ability for trauma cells and cerebral ischemia [9,10]. Such an action was evidenced by the significant inhibition of neuronal death [9], which is thought to proceed via a mechanism of action similar to a tyrosinase inhibition [10]. From this point of view, ORVT possesses a medicinal potential and a therapeutic value that might be exploited in medicine or as a food complement [11,12].

The stilbenoid group is known to undergo *trans*/*cis* isomerization which can be achieved by either heat or UV-light irradiation. Despite, the *t*-isomeric form of stilbenoid is thermodynamically more stable than the *c*-form, the thermal isomerization in both directions requires, in general, relatively high temperatures as part of the properties of stilbenoids documented in an earlier comprehensive review [13].

The description of ORVT's photokinetics has not yet been made available in the literature. It has however been quantitatively established that it undergoes a *trans-cis* photoisomerization in organic media [13] (Scheme 1). The photochemical data available on close analogue molecules, indicated that stilbenoids obeyed a relatively fast (28 ps) singlet-state dominated *trans-cis* photoisomerization in organic solvents [13]. In terms of photoreactivity in solution, *t*-resveratrol (*t*-RVT) [14,15], for instance, phototransforms faster into the *c*-form when the whole range of UV-VIS is used compared to a UV-irradiation at 254 nm. Nonetheless, *t*-RVT also reacts to irradiation with visible light (400–600 nm) yet in a slower transformation despite the fact that its electronic absorption spectrum does not exceed 360 nm [14].

In terms of kinetic data analysis, first-order kinetics was the basic tool used to calculate photoreactions' rate-constants and quantum yields of stilbenoids such as resveratrols [13,14]. Interestingly, it has been reported that the *t*-RVT rate-constant increased with irradiation wavelength [14].

It is however important to underline that the description of photoreactions by thermal kinetics (such as first-order kinetics) is not adequate since the latter models ignore the contribution of light to the mathematical equations [16–18]. In this respect, the Φ-order kinetics is a much better tool to rationalise the behaviour and to reliably quantify photoreactions' parameters such as quantum yields.

In this study we present, for the first time, a new method to analyse the photokinetic data relative to *trans-cis* photoisomerization driven by

* Corresponding author.
E-mail address: mmaafi@dmu.ac.uk (M. Maafi).

http://dx.doi.org/10.1016/j.saa.2017.06.067
1386-1425/

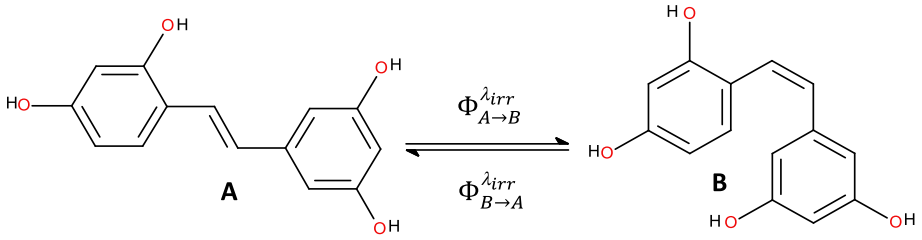

Scheme 1. Reversible photoisomerization of *t*-ORVT (A) and *c*-ORVT (B).

non-isosbestic UV or visible irradiation and its application to ORVT kinetic analysis. The kinetic tool explores ORVT photodegradation percentages and its actinometric usefulness.

2. Materials and Methods

2.1. Material

Oxyresveratrol, (*E*)-2,3′,4,5′-Stilbenetetrol, 2,3′,4,5′-Tetrahydroxy-*trans*-stilbene, 4-[(1*E*)-2-(3,5-Dihydroxyphenyl) ethenyl]-1,3-benzenediol (ORVT) was purchased from Sigma Aldrich. Spectrophotometric grade ethanol was purchased from Fisher Scientific.

2.2. Monochromatic Continuous Irradiation

An Ushio1000 W xenon arc-lamp was used as a light source. The lamp was connected to a monochromator model 101. The excitation beam was guided by an optical fibre to impinge from the top of the quartz cuvette holding the sample. In this configuration, the excitation and the monitoring light beams were perpendicular to each other.

2.3. The In Situ Monitoring Systems

A diode array spectrophotometer (Agilent 8453) was equipped with a 1-cm cuvette sample holder and a Peltier system model Agilent 8453 for temperature control. The sample was kept at 22 °C, stirred continuously during the irradiation, and completely sheltered from the ambient light.

A radiant power/energy meter model 70260 was used to quantify the radiant power of the monochromatic incident excitation beams.

2.4. HPLC Measurements

The HPLC system consisted of reversed-phase Waters symmetry (C18 150 mm × 3.9 mm 5 μm) column equipped with a PerkinElmer Series 200 pump, UV/Vis detector, vacuum degasser and a Perkin Elmer type Chromatography Interface 600 series Link linked to a computer system. The operating conditions included a mobile phase consisting of 85% water and 15% acetonitrile, a flow rate of 1.5 mL/min and a detection at 328 nm. The retention times of the species were 10.3 and 11.3 min, the calibration equation was $PA = 5\times10^{9}\times C - 59575$ with $r^2 = 0.996$, and a linearity range within the limits 4.7×10^{-4}–4.75×10^{-6}.

2.5. Oxyresveratrol Solutions

A 4.09×10^{-3} M stock solution of ORVT in ethanol was diluted to prepare fresh analytical solutions (ca. 2×10^{-5} M) for analysis. The flasks were protected from light by aluminium foil wrapping and were kept in the fridge.

All experiments were conducted at least in triplicates.

3. Result and Discussion

3.1. The Mathematical Background

3.1.1. General Equations

Φ–Order main equation model for the photoreversible transformation of compound (A) and photoproduct (B), which are driven by different forward ($\Phi^{\lambda_{irr}}_{A\to B}$) and reverse ($\Phi^{\lambda_{irr}}_{B\to A}$) quantum yields (Scheme 1), is given by Eq. (1) for a non-isosbestic and continuous irradiation at wavelength λ_{irr} where species A and B absorb differently ($\varepsilon^{\lambda_{irr}}_A \neq \varepsilon^{\lambda_{irr}}_B$) the incident light ($P_{\lambda_{irr}}$) [19].

$$A^{\lambda_{irr}/\lambda_{obs}}_{tot}(t) = A^{\lambda_{irr}/\lambda_{obs}}_{tot}(pss) + \frac{A^{\lambda_{irr}/\lambda_{obs}}_{tot}(0) - A^{\lambda_{irr}/\lambda_{obs}}_{tot}(pss)}{A^{\lambda_{irr}/\lambda_{irr}}_{tot}(0) - A^{\lambda_{irr}/\lambda_{irr}}_{tot}(pss)} \times \frac{l_{\lambda_{obs}}}{l_{\lambda_{irr}}} \times \log\left[1 + \left(10^{\left[\left(A^{\lambda_{irr}/\lambda_{irr}}_{tot}(0) - A^{\lambda_{irr}/\lambda_{irr}}_{tot}(pss)\right)\times\frac{l_{\lambda_{irr}}}{l_{\lambda_{obs}}}\right]} - 1\right) \times e^{-k^{\lambda_{irr}}_{A\rightleftharpoons B}\times t}\right] \quad (1)$$

In Eq. (1), $l_{\lambda_{irr}}$ and $l_{\lambda_{obs}}$ are independent (non-equal) quantities corresponding respectively to the optical path lengths of the irradiation and monitoring beams inside the sample. $A^{\lambda_{irr}/\lambda_{obs}}_{tot}$ is the measured total absorbance of the medium along $l_{\lambda_{obs}}$ and at the observation wavelength (λ_{obs}), at the initial time (t = 0), at time t and at the photostationary state, pss (t = ∞). Log is the base 10 logarithm.

The exponential factor, representing the overall rate-constant $k^{\lambda_{irr}}_{A\rightleftharpoons B}$ that can be obtained by fitting the kinetic trace to Eq. (1), has the following analytical expression (Eq. (2)),

$$k^{\lambda_{irr}}_{A\rightleftharpoons B} = \left(\Phi^{\lambda_{irr}}_{A\to B}\times\varepsilon^{\lambda_{irr}}_A + \Phi^{\lambda_{irr}}_{B\to A}\times\varepsilon^{\lambda_{irr}}_B\right)\times l_{\lambda_{irr}}\times P_{\lambda_{irr}}\times F_{\lambda_{irr}}(pss) = \beta_{\lambda_{irr}}\times P_{\lambda_{irr}} \quad (2)$$

with $\beta_{\lambda_{irr}}$ represents the pseudo-rate constant and the factor $F_{\lambda_{irr}}(pss)$ is the time-independent photokinetic factor, given by

$$F_{\lambda_{irr}}(pss) = \frac{1-10^{-\left(A^{\lambda_{irr}/\lambda_{irr}}_{tot}(pss)\times l_{\lambda_{irr}}/l_{\lambda_{obs}}\right)}}{A^{\lambda_{irr}/\lambda_{irr}}_{tot}(pss)\times l_{\lambda_{irr}}/l_{\lambda_{obs}}} \quad (3)$$

3.1.2. The Elucidation Method

In order to avoid degeneracy of the kinetic solution [17,20,21], an elucidation method capable of delivering the true set of values for the reaction unknowns which for a photoreversible reaction such as that observed for ORVT photoisomerization, are the forward ($\Phi^{\lambda_{irr}}_{A\to B}$) and the reverse ($\Phi^{\lambda_{irr}}_{B\to A}$) quantum yields, in addition to the absorption coefficient of the photoproduct ($\varepsilon^{\lambda_{irr}}_B$ of *c*-ORVT). We propose for the first time in this work a method exclusively based on non-isosbestic irradiation.

This elucidation method can be realised in three steps. (i) The first step involves the determination of the concentration ($C_A(pss)$) of the initial species (A or *t*-ORVT in Scheme 1) at the pss by monitoring its photodegradation reaction performed under a non-isosbestic irradiation at a given λ_{irr}, using HPLC. The concentration of photoproduct at the photostationary state ($C_B(pss)$) is worked out from the mass balance equation as, $C_B(pss) = C(0) - C_A(pss)$. (ii) The second step involves

reconstructing the photoproduct's absorption spectrum ($\varepsilon_B^{\lambda_{irr}}$) using Eq. (4).

$$\varepsilon_B^{\lambda_{irr}} = \frac{A_{tot}^{\lambda_{irr}/\lambda_{obs}}(pss) - C_A(pss) \times \varepsilon_A^{\lambda_{irr}} \times l_{\lambda_{obs}}}{(C(0) - C_A(pss)) \times l_{\lambda_{obs}}} \quad (4)$$

In the final step, (iii) the absolute values for $\Phi_{A\to B}^{\lambda_{irr}}$ and $\Phi_{B\to A}^{\lambda_{irr}}$ at any irradiation wavelength can be derived from Eqs. (5a) and (5b).

$$\Phi_{A\to B}^{\lambda_{irr}} = \frac{\upsilon_0^{\lambda_{irr}/\lambda_{obs}}}{\left(\varepsilon_B^{\lambda_{irr}} - \varepsilon_A^{\lambda_{irr}}\right) \times l_{\lambda_{obs}} \times \varepsilon_A^{\lambda_{irr}} \times l_{\lambda_{irr}} \times P_{\lambda_{irr}} \times F_{\lambda_{irr}}(0) \times C_0} \quad (5a)$$

$$\Phi_{B\to A}^{\lambda_{irr}} = \frac{1}{\varepsilon_B^{\lambda_{irr}}}\left[\frac{k_{A\rightleftharpoons B}^{\lambda_{irr}}}{l_{\lambda_{irr}} \times P_{\lambda_{irr}} \times F_{\lambda_{irr}}(pss)} - \Phi_{A\to B}^{\lambda_{irr}} \times \varepsilon_A^{\lambda_{irr}}\right] \quad (5b)$$

Eq. (5a) is obtained by rearranging the equation (Eq. (6a)) of the reaction initial velocity ($\upsilon_0^{\lambda_{irr}/\lambda_{obs}}$), whose numerical value can be worked out from Eq. (6b) that has been derived by differentiation of Eq. (1).

$$\upsilon_0^{\lambda_{irr}/\lambda_{obs}} = \left(\varepsilon_B^{\lambda_{irr}} - \varepsilon_A^{\lambda_{irr}}\right) \times l_{\lambda_{obs}} \times \Phi_{A\to B}^{\lambda_{irr}} \times \varepsilon_A^{\lambda_{irr}} \times l_{\lambda_{irr}} \times P_{\lambda_{irr}} \times F_{\lambda_{irr}}(0) \times C_A(0) \quad (6a)$$

with $F_{\lambda_{irr}}(0)$ calculated using Eq. (3) where $A_{tot}^{\lambda_{irr}/\lambda_{irr}}(t)$ was set to equal $A_{tot}^{\lambda_{irr}/\lambda_{irr}}(0)$.

$$\upsilon_0^{\lambda_{irr}/\lambda_{obs}} = \left(\frac{dA_{tot}^{\lambda_{irr}/\lambda_{obs}}}{dt}\right)_0 = \frac{A_{tot}^{\lambda_{irr}/\lambda_{obs}}(0) - A_{tot}^{\lambda_{irr}/\lambda_{obs}}(pss)}{A_{tot}^{\lambda_{irr}/\lambda_{irr}}(0) - A_{tot}^{\lambda_{irr}/\lambda_{irr}}(pss)} \times \frac{k_{A\rightleftharpoons B}^{\lambda_{irr}}(mod.)}{Ln(10) \times l_{\lambda_{irr}}/l_{\lambda_{obs}}} \times \left(10^{\left[\left(A_{tot}^{\lambda_{irr}/\lambda_{irr}}(pss) - A_{tot}^{\lambda_{irr}/\lambda_{irr}}(0)\right) \times l_{\lambda_{irr}}/l_{\lambda_{obs}}\right]} - 1\right) \quad (6b)$$

This methodology, presented here for the first time, circumvent the exclusive requirement of an isosbestic irradiation offered by the previous approach [19]. In this sense, the present method not only widens the applicability of the kinetic elucidation to the entire spectrum of the absorbing photoreversible species (ORVT has only three isosbestic points in a 200-nm absorption span, Fig. 1) but also reduces the number of steps to be performed.

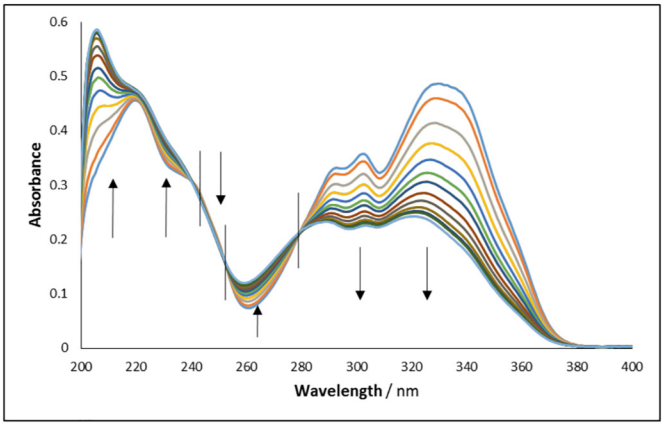

Fig. 1. Example of consecutive electronic absorption spectra of 2×10^{-5} M ORVT in ethanol solution subjected to continuous and monochromatic irradiation at 328 nm (total irradiation time of 2.6×10^3 s at radiant power of $P_{328} = 2.64 \times 10^{-7}$ einsteins^{-1} dm^{-3}). The arrows indicate the absorption change during photoreaction whereas the vertical line corresponds to the isosbestic points.

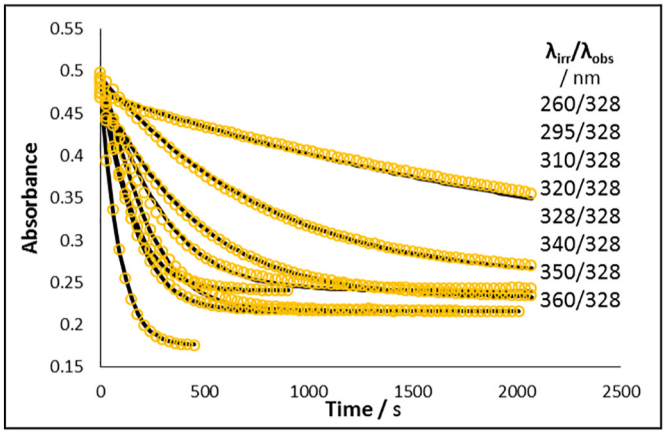

Fig. 2. Photokinetic traces of ORVT in ethanol solution (2×10^{-5} M) at $\lambda_{irr} = 260, 280, 310, 328, 350$ and 370 nm and $\lambda_{obs} = 328$ nm. The circles represent the experimental data whereas the lines represent the fitting traces using Eq. (1).

3.1.3. The Degradation Percentage

The knowledge of the quantum yields and the absorption coefficients of both species at any irradiation wavelength, as determined in the previous section, allows the determination of the thermodynamic equilibrium constant ($K_{\rightleftharpoons}^{\lambda_{irr}}$) of the reaction for the selected irradiation wavelength as given by Eq. (7).

$$K_{\rightleftharpoons}^{\lambda_{irr}} = \frac{\Phi_{A\to B}^{\lambda_{irr}} \times \varepsilon_A^{\lambda_{irr}}}{\Phi_{B\to A}^{\lambda_{irr}} \times \varepsilon_B^{\lambda_{irr}}} = \frac{C_B(pss)}{C_A(pss)} \quad (7)$$

Therefore, using the mass balance, the concentration of the initial compound (Eq. (8)) is calculated for any irradiation wavelength without the need for further HPLC analyses.

$$C_A(pss) = \frac{C_A(0)}{K_{\rightleftharpoons}^{\lambda_{irr}} + 1} \quad (8)$$

The degradation percentage of species A at a given irradiation wavelength is then given by

$$\text{Degradation}\% = 100 - C_A(pss)\% = 100 - \frac{C_A(pss)}{C_A(0)} \times 100 \quad (9)$$

3.2. ORVT Photodegradation and Φ-Order Reaction

The electronic spectra of ORVT isomers are characterised by two major bands in the 200–250 and 250–400 nm with the main maximum situated at 328 nm ($\log\varepsilon = 4.45$). These bands are attributed to π,π* transitions corresponding to the extended π system in ORVT which might overlay a minor contribution of n,π* transitions due to the presence of hydroxyl groups [13]. This spectral pattern was generally observed for stilbenoids, where the electronic donor effects of the hydroxyls on both benzenic groups of ORTV induced a bathochromic shift of the spectrum (~48 nm) compared to *t*-stilbene [13].

Table 1
Overall photoreaction rate-constant, spectroscopic and kinetic parameter values of ORVT for a set of monochromatic irradiations performed in ethanol at 22 °C.

λ_{irr}/nm	$A_{tot}^{\lambda_{irr}/328}(0)$	$A_{tot}^{\lambda_{irr}/\lambda_{irr}}(pss)$	$P_{\lambda_{irr}} \times 10^7$/einstein s^{-1} dm^{-3}	$k_{A\rightleftharpoons B}^{\lambda_{irr}}$/s^{-1}
260	0.474	0.222	1.79	0.0004
295	0.492	0.270	2.52	0.0015
310	0.474	0.219	2.10	0.0025
320	0.489	0.240	5.41	0.0085
328	0.486	0.240	2.39	0.0047
340	0.498	0.216	2.83	0.0068
350	0.480	0.215	3.21	0.0080
360	0.468	0.175	4.60	0.0150

Table 2
Spectrophotometric and experimental parameters of ORVT reaction performed at $\lambda_{irr} = \lambda_{obs} = 328$ nm and 22 °C. The variation of the initial species concentration was monitored by HPLC as presented in Fig. 3.

$\Delta C \times 10^5$/M	$A_{tot}^{328/328}(0)$	$A_{tot}^{328/328}(pss)$	ε_A^{328}/M^{-1} cm^{-1}	l_{obs} /cm	l_{irr} /cm	$F_{328}(0)$	$F_{328}(pss)$	$P_{328} \times 10^7$/einstein s^{-1} dm^{-3}
1.68	0.565	0.269	28,261.8	1	2.01	0.816	1.317	2.76

The temporal evolution of the spectrophotometric spectra obtained under continuous monochromatic irradiation (Fig. 1) of the ethanolic solutions of *t*-ORVT (Scheme 1) was characterised by two main features. The appearance of a new peak at 205 nm, adjacent to the B-band at 220 nm [13] which itself was not significantly affected during the phototransformation, and a significant decrease in absorbance of the long wavelength band (280–400 nm). Three isosbestic points were observed on the consecutive spectra at 240, 253 and 279 nm. These features strongly suggest that the phototransformation occurs quantitatively without by-products, in less than an hour. The variation of the spectra was exclusively due to a photoreaction because in the dark (but otherwise in the same experimental conditions) *t*-ORVT is found to be thermally stable at 22 °C for long periods (>4 h). These results also suggest that the isomerization is the only photoreaction taking place under our experimental conditions. The possible photocyclisation of *c*-ORVT is discarded because usually the electronic spectrum of the closed isomer is much different from those of the *c*- and *t*-stilbenoids (the produced dihydrophenanthrene absorbs in the visible region (>400 nm) of the spectrum [22], a missing feature on ORVT spectra performed in our experimental conditions).

Kinetic traces were recorded at selected irradiation wavelengths that cover most of the absorption spectrum of ORVT (λ_{irr} = 260, 280, 310, 328, 350 and 360 nm). These traces were fitted with Eq. (1) for various observation wavelengths; we present a sample of kinetic traces in Fig. 2 where a unique observation (λ_{obs} = 328 nm) was used for comparison purposes.

As can be seen, good fittings with Eq. (1) were obtained for all traces (Fig. 2). These results confirm that both ORVT obeys Φ-order kinetics and Scheme 1 is reliable.

The *trans-cis* overall rate-constant values ($k_{A \rightleftharpoons B}^{\lambda_{irr}}$) of ORVT photodegradation reaction were determined as the fitting parameter (Table 2). The $k_{A \rightleftharpoons B}^{\lambda_{irr}}$ values increased steadily from 260 to 350 nm but decreased beyond. However, according to Eq. (2), the experimental values of $k_{A \rightleftharpoons B}^{\lambda_{irr}}$ should be considered with care as the overall rate-constant depends on both reaction attributes ($\varepsilon_A^{\lambda_{irr}}$, $\varepsilon_B^{\lambda_{irr}}$, $\Phi_{A \rightarrow B}^{\lambda_{irr}}$ and $\Phi_{B \rightarrow A}^{\lambda_{irr}}$) and experimental conditions ($l_{\lambda_{irr}}$, $P_{\lambda_{irr}}$ and $C_A(0)$). The former parameters should be assumed wavelength-dependent, and the latter ones are variable between experiments. Hence, the numerical values of Φ-order $k_{A \rightleftharpoons B}^{\lambda_{irr}}$ have a meaning only for the particular conditions of the experiment at hand and the nature of the analysed compound. Therefore, $k_{A \rightleftharpoons B}^{\lambda_{irr}}$ values are not useful for comparison between different experiments performed on the same compound. This statement includes the cases when only the irradiation wavelength is different (Table 2), experiments involving different compounds, let alone experiments employing polychromatic light for irradiation. It is important to underline that the radiant power ($P_{\lambda_{irr}}$) represents the most difficult parameter to tune between different experiments. In this respect, it is recommended to determine all the fundamental parameters prior to proceeding with comparison.

The discussion above is even more acutely relevant when the kinetic data treatments use classical/thermal order kinetics since in such a case, the determined rate-constants lack any fundamental physical meaning for photoreactions.

3.3. Example of Unidentifiability Issues

The identifiability issue is raised whenever a degeneracy of the kinetic solution is observed as a direct consequence of a lack of information [20,21,23,24]. The identifiability is an issue for reaction kinetics whenever it is possible to propose different sets of plausible values (kinetic solutions) for the set of the reaction's unknowns. This is the case when

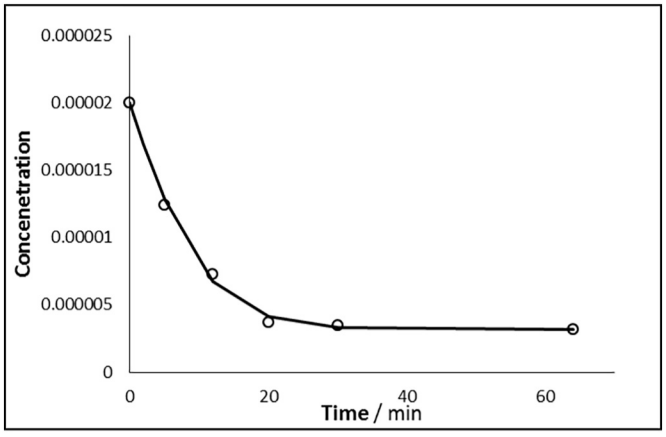

Fig. 3. Evolution of *t*-ORVT concentration ($C_A(0) = 2 \times 10^{-5}$ M, $C_A(pss) = 3.2 \times 10^{-6}$ M) monitored by HPLC when irradiated continuously with a monochromatic beam at 328 nm (2.39×10^{-7} einstein s^{-1} dm^{-3}, 22 °C) and fitted by Eq. (10a). The circles correspond to experimental data whereas the line represents Eq. (10a) that has been fed with the data of case # 1 in Table 3.

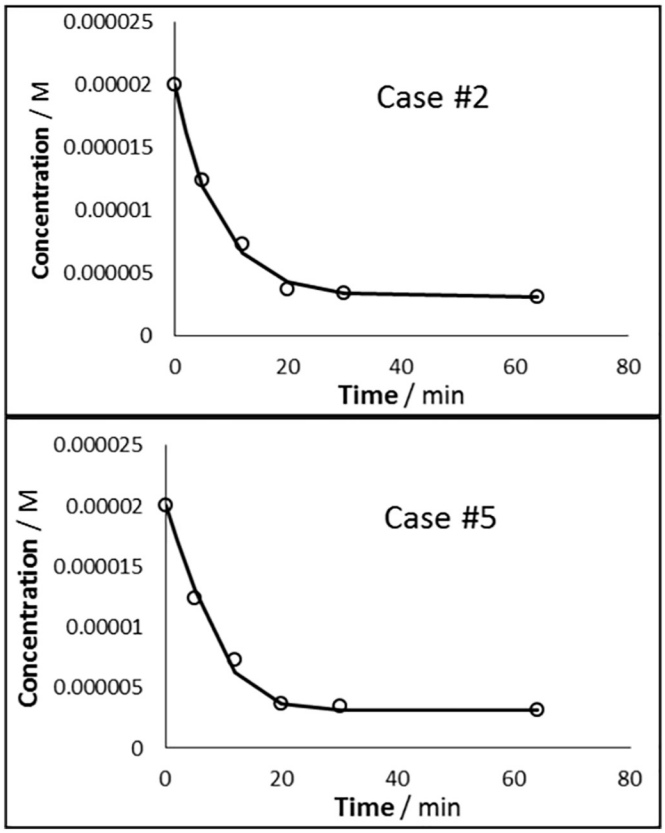

Fig. 4. Examples of good fitting of the experimental values of *t*-ORVT concentrations (circles, as shown in Fig. 3) by Eq. (10a) using the data of Table 3 corresponding to cases # 2 and 5 (lines).

Table 3
Examples of fitting parameters and calculated unknowns for the reaction of ORVT in ethanol.

Case #→		1	2	3	4	5	6	7
Parameters[a]↓								
Fitting	α[b]	35,391.74	2525	25,586	49,256	53,145	55,351	57,124
	$k_{A\rightleftharpoons B}^{\lambda_{irr}}$[b]	0.005	0.0023	0.003	0.0031	0.0033	0.0037	0.0037
Unknowns	$\varepsilon_B^{\lambda_{irr}}$	10,653.97	27,005.58	15,532.45	3756.33	1821.51	723.99	−158.09
	$\Phi_{AB}^{\lambda_{irr}}$	0.23	0.13	0.17	0.17	0.19	0.21	0.21
	$\Phi_{BA}^{\lambda_{irr}}$	0.21	0.025	0.057	0.24	0.54	1.50	−6.89

[a] $\varepsilon_B^{\lambda_{irr}}$ (in M^{-1} cm^{-1}) was calculated using Eq. (10b) for cases # 2–7.
[b] α and $k_{A\rightleftharpoons B}^{\lambda_{irr}}$ expressed in M^{-1} and s^{-1}, respectively.

considering a reactive system's kinetic data or even a single kinetic trace of that reactive system. Each of the distinct solutions provides an excellent fitting of the experimental data and therefore the knowledge of the true solution (among the set of these plausible solutions) becomes impossible. We show hereafter an illustration example of identifiability for the case of ORVT.

Let's consider the data obtained by HPLC (Fig. 3) that correspond to the progressive depletion of *t*-ORVT concentration in the reactive medium through time, up to the pss. These data also provide the values for the initial and pss concentrations of ORVT (i.e. $C_A(0)$ and $C_A(pss)$, respectively).

The formula that describes this reaction kinetic can be obtained by rearranging Eq. (1) and combining it with the mass balance.

$$C_A(t) = C_A(pss) + \frac{1}{\alpha}\mathrm{Log}\left[1 + \left(10^{\alpha\times\Delta C} - 1\right) \times e^{-k_{A\rightleftharpoons B}^{\lambda_{irr}}\times t}\right] \quad (10a)$$

Eq. (10a) is written here as dependent on two parameters α and $k_{A\rightleftharpoons B}^{\lambda_{irr}}$ ($\Delta C = C_A(0) - C_A(pss)$), where the latter corresponds to Eq. (2) whereas the former parameter is given by;

$$\alpha = \left(\varepsilon_A^{\lambda_{irr}} - \varepsilon_B^{\lambda_{irr}}\right) \times l_{\lambda_{irr}} \quad (10b)$$

The definition of these two parameters will allow the determination of the three reaction unknowns, namely $\varepsilon_B^{\lambda_{irr}}$, $\Phi_{A\rightarrow B}^{\lambda_{irr}}$ and $\Phi_{B\rightarrow A}^{\lambda_{irr}}$ derived from Eqs. (10b), (10c) and (10d), respectively.

$$\Phi_{A\rightarrow B}^{\lambda_{irr}} = \frac{C_B(pss) \times k_{A\rightleftharpoons B}^{\lambda_{irr}}}{\varepsilon_A^{\lambda_{irr}} \times l_{\lambda_{irr}} \times P_{\lambda_{irr}} \times F_{\lambda_{irr}}(pss) \times C_0} \quad (10c)$$

$$\Phi_{B\rightarrow A}^{\lambda_{irr}} = \frac{C_A(pss) \times k_{A\rightleftharpoons B}^{\lambda_{irr}}}{\varepsilon_B^{\lambda_{irr}} \times l_{\lambda_{irr}} \times P_{\lambda_{irr}} \times F_{\lambda_{irr}}(pss) \times C_0} \quad (10d)$$

The experimental conditions and spectrophotometric parameters of the reaction monitored by HPLC (Fig. 3) and subjected to non-isosbestic irradiation, are given in Table 2.

For the purposes of illustration of the identifiability problem, we assume that only Eqs. (10a)–(10d) are available (of course more equations have been derived to achieve an elucidation method as proposed in earlier sections). Hence, the above framework serves the fitting of the experimental HPLC data (Fig. 3) to Eq. (10a). The important question here is whether there is a unique set of parameters (α and $k_{A\rightleftharpoons B}^{\lambda_{irr}}$) that can be extracted from the curve fitting.

The treatment of the data according to model Eq. (10a) yields a great number (an infinity in theory) of very good fittings of the HPLC data (Fig. 4) which yield significantly different values for the reaction's basic unknowns ($\varepsilon_B^{\lambda_{irr}}$, $\Phi_{A\rightarrow B}^{\lambda_{irr}}$ and $\Phi_{B\rightarrow A}^{\lambda_{irr}}$) due the fact that the worked out fitting parameters (α and $k_{A\rightleftharpoons B}^{\lambda_{irr}}$) for each case are substantially different from case to case (Table 3).

This proves that using valid equations (Eqs. (10a)–(10d)) is not in itself sufficient to perform a complete kinetic analysis since here it is possible to obtain a series of plausible solutions. This degeneracy cannot also be solved by only taking the "good fit" of the experimental data to an equation as the unique criterion. Among the solutions proposed in Table 3, some cases (# 6 and 7) fit well the experimental data however they yield physically meaningless (negative or $\Phi_{A\rightarrow B}^{\lambda_{irr}} > 1$) values for the unknowns and hence have to be discarded. Others (cases # 2–5) generate plausible values for the unknowns. Because these values are different but plausible, they represent a typical case of unidentifiability. It is important to underline that all these results found for the unknowns for cases # 2–5, do not conform with the true solution (case # 1) that was obtained by our elucidation method (vide infra Table 4).

This strongly indicates that despite the basic equations (Eqs. (10a)–(10d)) are perfectly valid and a good fit was found for each case, there is still confusion about what the true solution might be.

The degenerate solution (cases # 1–5) represents practically an acute challenge for the identification of the true solution. The identifiability problems exist, in its general terms, as well for thermal reaction kinetics. It is important to stress here that the identifiability problem exists as well when classical treatments based on 0th-, 1st- and 2nd-order kinetics are applied to photodegradation reactions but in addition to the issue of identifiability, there is the more important issue of the validity of the latter mathematical models (which are not suitable) for photoreactions. Therefore, not only it is recommended to use Φ-order kinetics for such studies but it is also mandatory to develop an elucidation method to solve uniquely the kinetics. The above discussion is also pertinent if the absorbance traces (such as those presented in Fig. 2) were used instead of the concentration profiles (Fig. 3).

3.4. Elucidation of ORVT Kinetics

The elucidation method proposed in Section 3.1.2 was used here to evaluate the kinetic parameters of ORVT.

Table 4
Quantum yields, overall rate-constant, absorption coefficients and initial velocity values for ORVT photodegradation reactions under different monochromatic irradiations.

λ_{irr}/nm	$P_{\lambda_{irr}}\times10^7$/einsteins^{-1} dm^{-3}	$A_{tot}^{\lambda_{irr}}(pss)$	$k_{A\rightleftharpoons B}^{\lambda_{irr}}$/$s^{-1}$	$v_0^{\lambda_{irr}}\times10^4$/$s^{-1}$	$\varepsilon_A^{\lambda_{irr}}$/$M^{-1}$ cm^{-1}	$\varepsilon_B^{\lambda_{irr}}$/$M^{-1}$ cm^{-1}	$F_{\lambda_{irr}}(0)$	$(\Phi_{A\rightarrow B}^{\lambda_{irr}} \pm SD)\times10^2$	$(\Phi_{B\rightarrow A}^{\lambda_{irr}} \pm SD)\times10^2$
260	1.95	0.097	0.00028	0.13	3137.99	7239.39	2.03	6.90 ± 0.86	2.30 ± 1.02
295	2.25	0.227	0.0016	−1.29	18,858.67	11,834.99	1.18	10.50 ± 0.17	4.30 ± 0.42
310	2.29	0.232	0.0026	−1.84	18,800.78	12,053.62	1.21	15.40 ± 1.32	9.10 ± 1.72
320	4.68	0.252	0.009	−11.17	25,047.97	12,150.87	0.99	21.34 ± 0.14	13.97 ± 0.11
328	2.01	0.239	0.005	−7.35	28,261.80	10,654.78	0.92	23.30 ± 1.57	21.91 ± 3.21
340	4.02	0.148	0.015	−23.44	26,490.31	7110.86	1.01	35.01 ± 1.32	26.34 ± 5.77
350	4.55	0.096	0.015	−21.94	17,801.98	3912.45	1.16	43.80 ± 1.60	26.26 ± 1.4
360	7.64	0.031	0.015	−14.94	9783.39	1690.81	1.61	45.38 ± 0.67	6.87 ± 1.6

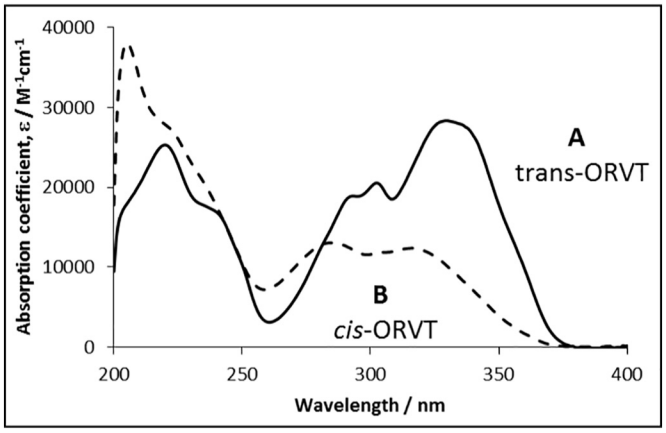

Fig. 5. Native and reconstructed electronic absorption spectra (absorption coefficient units) of *t*-ORVT and its *cis*-isomer photoproduct, respectively.

HPLC monitoring of the evolution of ORVT concentration during a selected non-isosbestic irradiation at 328 nm (Fig. 3), allowed the determination of the initial and pss concentrations as 2×10^{-5} M and 3.2×10^{-6} M, respectively.

The absorption spectrum of the photoproduct ($\varepsilon_B^{\lambda_{irr}}$) was then reconstructed using both Eq. (4) and the absorption spectrum of the reaction medium at pss (the reconstruction is carried out without physically separating *c*-ORVT from the reaction medium), Fig. 5.

The overall vibrational shape of *c*-ORVT spectrum is identical to that recorded for its photoisomer with variable absorption values, in agreement with the general pattern observed for stilbenoids [13]. These features also support the occurrence of the photoisomerization without any further degradation processes, as indicated in Scheme 1.

Once the absorption coefficients of the photoproduct are known, the determination of the individual absolute values of the quantum yield at any irradiation wavelength was achieved by using Eqs. (5a) and (5b) together with the numerical value of the reaction initial velocity (v_0) that can be calculated by Eqs. (6a) and (6b).

Both forward and reverse quantum yields have been found to depend on the irradiation wavelength (Table 4). 6.6- and 11.4-fold increases were recorded for $\Phi_{A\to B}^{\lambda_{irr}}$ and $\Phi_{B\to A}^{\lambda_{irr}}$ values, respectively, in the 260–350 nm range (Table 4). The values of the reverse quantum yield were always smaller than those observed for the forward reaction and the ratio of quantum yield values, ranging between 1 and 3, correlated linearly in an inverse proportionality relationship with the irradiation wavelength ($\Phi_{A\to B}^{\lambda_{irr}}/\Phi_{B\to A}^{\lambda_{irr}} = -0.0246 \times \lambda_{irr} + 9.44$, $r = 0.95$, in the range 260–350 nm).

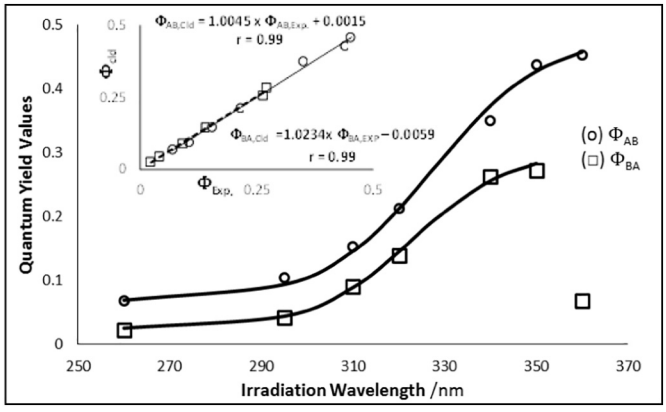

Fig. 6. Sigmoid patterns (Eqs. (11a) and (11b)) obeyed by the experimental quantum yield ($\Phi_{A\to B_{irr}}$ and $\Phi_{B\to A_{irr}}$) values of both ORTV isomers as experimentally measured for various irradiation wavelengths. Inset: linear relationship of the experimental and calculated (Eqs. (11a) and (11b)) values of $\Phi_{A\to B_{irr}}$ and $\Phi_{B\to A_{irr}}$.

Table 5
Concentrations of the species, thermodynamic equilibrium constants at pss and photodegradation percentage of *t*-ORVT at various irradiation wavelengths.

λ_{irr}/nm	$C_A(0)\times10^5$/M	$C_A(pss)\times10^6$/M	$C_B(pss)\times10^5$/M	$K_{eq}^{\lambda_{irr}}$	% degradation
260	1.79	7.83	1.003	1.28	56.17
295	1.74	3.54	1.36	3.92	79.67
310	1.69	4.65	1.22	2.63	72.47
320	1.74	4.21	1.32	3.15	75.90
328	1.6	4.19	1.18	2.82	73.83
340	1.61	2.7	1.34	4.95	83.20
350	1.91	2.23	1.69	7.59	88.36
360	1.68	0.43	1.64	38.23	97.45

It is also interesting to notice that the evolution of the quantum yields' values with λ_{irr} is well described by sigmoid functions (Fig. 6, Eqs. (11a) and (11b)), and a linear correlation is found between the calculated ($\Phi_{cld.}$) and experimental ($\Phi_{exp.}$) quantum yield values (inset of Fig. 6).

$$\Phi_{A\to B}^{\lambda_{irr}} = 0.068 + \frac{0.417}{1 + 440 \times e^{-0.0826(\lambda_{irr}-254)}} \quad (11a)$$

$$\Phi_{B\to A}^{\lambda_{irr}} = 0.025 + \frac{0.28}{1 + 135 \times e^{-0.0925(\lambda_{irr}-270)}} \quad (11b)$$

One of the advantages of our method is offered by Eqs. (11a) and (11b) that allow the determination of the quantum yield values for both isomers at any irradiation wavelength, in the spectral section 260–350 nm, based on the knowledge of only a few experimental values. The overall similarity between the sigmoid functions (Fig. 6) was also indicated by a good linear correlation established between the two sets quantum yield values ($\Phi_{A\to B}^{\lambda_{irr}} = 0.922 \times \Phi_{B\to A}^{\lambda_{irr}} + 0.043$, $r = 0.97$, between 260 and 340 nm).

The above findings suggest that the photodegradation of ORVT is mainly driven by UVA light (>310 nm). The quantum yield values (0.02–0.45 in ethanol) are within the range of values reported for stilbenes (0.48–0.32, for stilbene in methanol at 313 nm [25]). The reverse reaction ($\Phi_{B\to A}^{\lambda_{irr}}$) was relatively less photoreactive over irradiation than its counterpart in agreement with the general trend observed for stilbenoids and azobenzenes [13,26]. The variation of the quantum yield ratio with irradiation proves that the photoisomers' exited-states might be significantly different, which does not support the hypothesis that the decay of both isomers originates from a common intermediate. Indeed, it has been postulated that a twisted ($\theta = 90$) intermediate occurs, irrespective of irradiation wavelength, at the bottle neck region situated between excited-state and ground-state potential energy surfaces [27]. In this interpretation, the quantum yields of the *trans* and *cis*

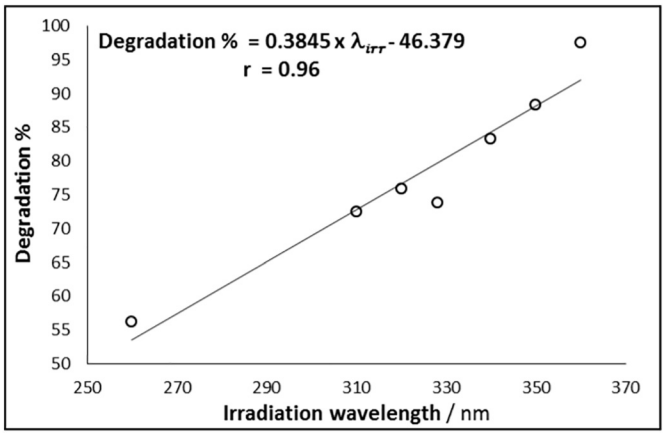

Fig. 7. Correlation between *t*-ORVT photodegradation % at pss and irradiation wavelength (λ_{irr}).

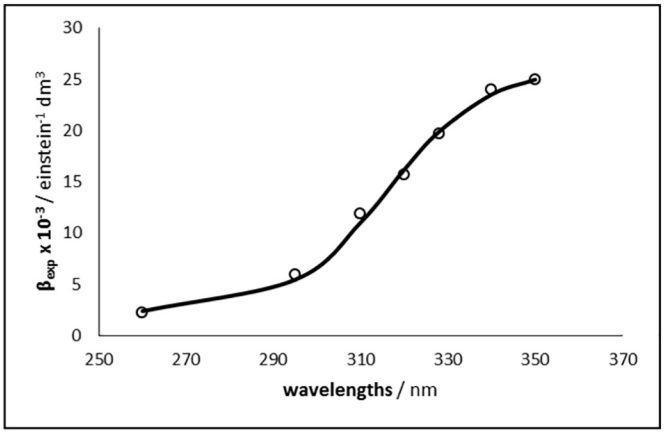

Fig. 8. Calculated β_{irr} values (circles) using Eq. (2) and the values of $k_{A \rightleftharpoons B_{irr}}$ and P_{irr} provided in Table 1. The fitting of the experimental data was drawn by the sigmoid model Eq. (12) (line).

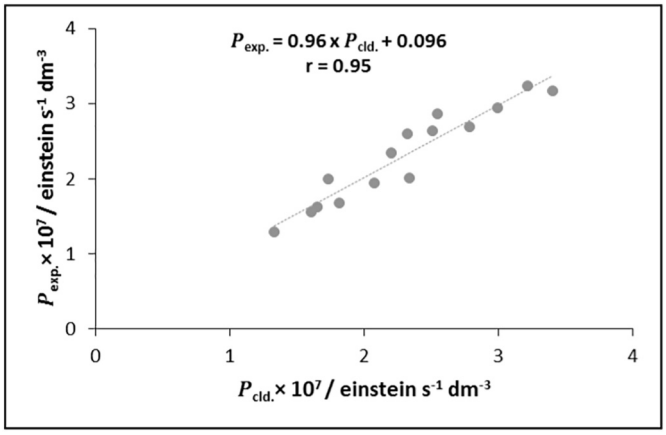

Fig. 10. Linear correlation of experimental ($P_{exp.}$) with calculated ($P_{cld.}$) values of the radiant power for wavelengths between 310 and 350 nm.

isomers are expected to be equal in the absence of major sterical hindrance, as they decay from the same species [25] and/or at least their ratios should be constant with irradiation wavelength (as would be stipulated by Kasha's rule [28]). Such a hypothesis has not been confirmed by a large number of quantum yield experimental data published in the literature for a variety of stilbenoids. The determined values of quantum yields for the isomers of each particular stilbene derivative were, in general, not found to be equal or wavelength independent [13]. For example, the most largely studied trans-stilbene has a quantum yield of 0.48 and its isomers a value of 0.32 in the same experimental conditions [27]. The situation is even more evidenced as, for instance, the quantum yield of trans-stilbene has been reported to vary with irradiations (0.48 at 254 nm and 0.32 at 313 nm) [13,25]. However, at the best of our knowledge there are no systematic studies of the effects of irradiation on stilbenoids quantum yields available in the literature, even though there are many examples of wavelength-dependent quantum yields for a variety of molecules [25,26,29,30]. Similar sigmoid behaviour was also observed for a number E/Z photoisomerizations [26,31–33].

The above literature results, which are corroborated by those laid out in the present study, do not back the hypothesis relating to a common excited-state intermediate that occurs independently of the irradiation wavelength. From a more general viewpoint, the wavelength dependence of the quantum yields corroborates the statement of Turro et al. [34] stipulating the non-universal applicability of Kasha's rule to photoreactions. If there is still no rational interpretation of this phenomenon

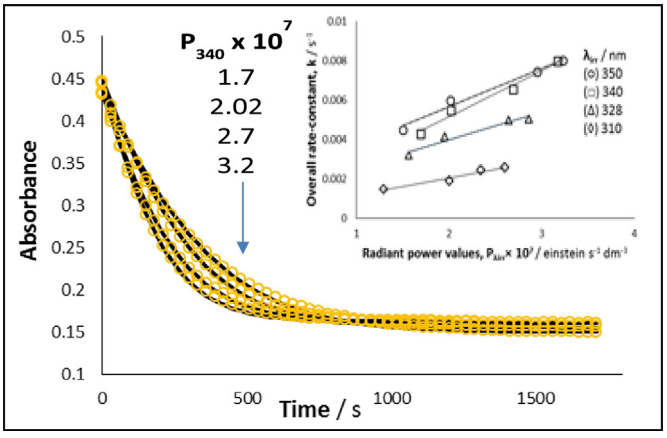

Fig. 9. Effect of increasing the radiant power of the monochromatic irradiation beam (at 340 nm) on the photokinetic traces of *t*-ORVT (2×10^{-5} M). The experimental data (circles) were fitted by Eq. (1). Inset: Linear correlation of $k_{A \rightleftharpoons B_{irr}}$ (in s^{-1}) with P_{irr} (in einstein s^{-1} dm^{-3}) for each wavelength.

a number of hypotheses have been proposed, which mainly relate to the existence of various excited states that may be due to different conformers [35].

The calculated percentage of photodegradation of *t*-ORVT in ethanol was found to range between 56 and 97% within the 260–360 nm spectral region (Table 5). Overall, the degradation percentage increases linearly with irradiation wavelength (Fig. 7). These results prove that the photoreaction favours the phototransformation of *t*-ORVT where *c*-ORVT has a major contribution to the pss species composition. This corroborates the lower quantum yields and absorption coefficient values of *c*-ORVT compared to those of the initial isomer. However, the high degradation percentages meant that exposure of ORVT to UVA and/or Visible light causes almost its complete depletion and therefore it is strongly recommended to shield it from light in all applications and manipulations. This would also justify raising some questions about the photostability of *t*-ORVT in vivo [36].

The method presented here would be useful for the study of phytomolecules/drugs that obey photoisomerization reactions and will contribute to fully characterise and rationalise their photokinetics and photostability with the aim of improving their safety and durability.

3.5. ORVT Actinometer

The actinometric potential of ORVT can be evaluated by using the data obtained on the photoreactivity of this species at different wavelengths. Using the data of Table 1, the values of the β factors can readily be calculated on the basis of Eq. (2). This methodology has the advantage to be much faster and simpler than the previously used approach [19]. When the β factors were graphically represented against the corresponding wavelengths, a sigmoid shape is obtained (Fig. 8, Eq. (12)).

$$\beta_{\lambda_{irr}} = 2220 + \frac{23900}{1 + 139 \times e^{-0.089 \times (\lambda_{irr} - 260)}} \quad (12)$$

The advantage of Eq. (12) is both to allow obtaining the β values at any wavelength in the range studied, and to facilitate the determination of the radiant power ($P_{\lambda_{irr,x}}$) of an unknown source if its monochromatic beam wavelength ($\lambda_{irr,x}$) is situated between 310 and 350 nm, the most useful part of photodegradation causative range of ORVT. This can be achieved by simply taking the ratio $P_{\lambda_{irr,x}} = k^{\lambda_{irr,x}}_{A \rightleftharpoons B} / \beta_{\lambda_{irr,x}}$, with these parameters correspond to the $\beta_{\lambda_{irr,x}}$ value calculated using Eq. (12) for $\lambda_{irr,x}$, and $k^{\lambda_{irr,x}}_{A \rightleftharpoons B}$ is obtained by irradiating a 2×10^{-5} M ORVT ethanolic solution (2.1 mL) by the considered beam (at $\lambda_{irr,x}$) and fitting its trace to Eq. (1).

In order to test the validity of this new procedure, the actinometric properties of ORVT have been evaluated on freshly prepared solutions that were subjected to irradiation (at λ_{irr} = 310, 328, 340 and 350 nm) using beams of different radiant powers (the rest of the experimental

parameters were otherwise kept the same). The selected value of $P_{\lambda_{irr}}$ in this study fit within the limits offered by of our instrument. For any given λ_{irr}, the experimental kinetic traces for the series of radiant power values (Fig. 9) were each fitted to the model Eq. (3). The observed good fitting further confirmed that ORTV obeys Φ-order kinetics.

For the purpose of this study, the various radiant power values of these experiments were considered unknown and were determined as stated above (using the determined Φ-order rate-constants for each irradiation). The reliability of the method is indicated by a good correlation between the experimental ($P_{cld.}$) and the calculated ($P_{\mathrm{exp.}}$) values of the radiant power (Fig. 10). The straight line is characterised by a slope close to unity and a small intercept.

The simplicity with which this method can be implemented as well as its reliability make it a good alternative to the actinometric methods provided in the literature [37]. More specifically for drugs, ORVT can stand as an alternative for the ICH recommended procedure that uses the controversial quinine hydrochloride actinometer [38–40]. ORVT actinometry would be also very useful for the study of the photostability of phytochromes absorbing in the range 310–350 nm. Finally, it is important to notice that to implement the actinometric method presented in this work, it is not required to know neither the absolute values of the forward and reverse quantum yields nor the produced photoisomers' spectrum. This arguably brings an improvement in actinometry procedure as our method, based on the $\beta_{\lambda_{irr}}$ factors, removes two of the most important criteria that were recommended for the development of actinometers [37,41].

4. Conclusion

The high photo-instability of ORVT in solution (up to 97%) enforces the recommendation that this compound should be shielded from light at all stages whether in production, formulation or in use conditions (especially in solution).

It seems that the quantum yield of trans/cis photoreversible systems should a priori be considered wavelength dependent, as indicated by the results of ORVT, but also other studies [25,26,29,30]. Therefore, the quantum yield values obtained using polychromatic irradiations, might be deemed misleading, as the quantum yield might not be constant over a spectral range covered by the polychromatic irradiation, and must be considered with care, as only an average value is obtained that does not hint to the possible fine tuning of the quantum yield values.

References

[1] J.I. Cacho, N. Campillo, P. Viñas, M. Hernández-Córdoba, J. Chromatogr. A 1315 (2013) 21–27.
[2] G.J. Fan, X.D. Liu, Y.P. Qian, Y.J. Shang, X.Z. Li, F. Dai, J.G. Fang, X.L. Jin, B. Zhou, Bioorg. Med. Chem. 17 (2009) 2360–2365.
[3] P. Lorenz, S. Roychowdhury, M. Engelmann, G. Wolf, T.F.W. Horn, Nitric Oxide Biol. Chem. 9 (2003) 64–76.
[4] P. Sasivimolphan, V.K. Lipipun, M. Takemoto, P. Pramyothin, M.K. Hattori, Antivir. Res. 84 (2009) 95–97.
[5] H. Oh, E.K. Ko, J.Y. Jun, M.H. Oh, S.U. Park, K.H. Kang, H.S. Lee, Y.C. Kim, Planta Med. 68 (2002) 932–934.
[6] H. Li, W.K.K. Wu, Z. Zheng, C.T. Che, Z.J. Li, D.D. Xu, C.C.M. Wong, C.G. Ye, J.J.Y. Sung, C.H. Cho, M. Wang, Eur. J. Pharmacol. 637 (2010) 55–61.
[7] Y.J. Chun, S. Kim, D. Kim, S.K. Lee, F.P. Guengerich, Cancer Res. 61 (2001) 8164–8170.
[8] T. Chuanasa, J. Phromjai, V. Lipipun, K. Likhitwitayawuid, M. Suzuki, P. Pramyothin, M. Hattori, K. Shiraki, Antivir. Res. 80 (2008) 62–70.
[9] K. Likhitwitayawuid, A. Sornsute, B. Sritularak, P. Ploypradith, Bioorg. Med. Chem. Lett. 16 (2006) 5650–5653.
[10] S. Song, H. Lee, Y. Jin, Y.M. Ha, S. Bae, H.Y. Chung, H. Suh, Bioorg. Med. Chem. Lett. 17 (2007) 461–464.
[11] C. Breuer, G. Wolf, S.A. Andrabi, P. Lorentz, T.F.W. Horn, Neurosci. Lett. 393 (2006) 113–118.
[12] P. Rodríguez-Bonilla, J.M., F. García-Carmona, J. Chromatogr. B 878 (2010) 1569–1575.
[13] H. Gorner, H.J. Kuhn, Cis-trans photoisomerization of stilbenes and stilbene-like molecules, in: D.C. Neckers, D.H. Volman, G. Von Bunau (Eds.), Advances in Photochemistry, 19, John Wiley & Sons, New York, Chichester, Brisbane, Toronto, Singapore, 1995.
[14] C.G. Silva, J. Monteiro, R.R. Marques, A.M. Silva, C. Martínez, M. Canle, J.L. Faria, Photochem. Photobiol. Sci. 12 (2013) 638–644.
[15] I. Džeba, T. Pedzinski, B. Mihaljević, J. Photochem. Photobiol. A Chem. 299 (2015) 118–124.
[16] M. Maafi, R.G. Brown, J. Photochem. Photobiol. A Chem. 187 (2007) 319–324.
[17] M. Maafi, Phys. Chem. Chem. Phys. 12 (2010) 13248–13254.
[18] W. Maafi, M. Maafi, Int. J. Pharm. 456 (2013) 153–164.
[19] M. Maafi, W. Maafi, Int. J. Pharm. 471 (2014) 536–543.
[20] M. Maafi, R.G. Brown, In. J. Chem. Kinet. 37 (2005) 717–727.
[21] M. Maafi, R.G. Brown, In. J. Chem. Kinet. 40 (2008) 268–281.
[22] K.A. Muszkat, E. Fischer, J. Chem. Soc. II (1967) 662–678.
[23] S. Vajda, H. Rabitz, J. Phys. Chem. 92 (1988) 701.
[24] K. Sienicki, G. Durocher, J. Photochem. Photobiol. A Chem. 63 (1992) 279.
[25] H. Suzuki, Bull. Chem. Soc. Jpn. 25 (1952) 145–150.
[26] G. Zimmerman, L.-Y. Chow, U.-J. Paik, J. Am. Chem. Soc. 80 (1958) 3528–3531.
[27] J. Malkin, Photophysical and Photochemical Properties of Aromatic Compounds, CRC Press, Boca Raton, 1992.
[28] M. Kasha, Discuss. Faraday Soc. 9 (1950) 14–19.
[29] M. Mazzoni, G. Agati, G.J. Troup, R. Pratesi, J. Opt. A Pure Appl. Opt. 5 (2003) S374–S380.
[30] O.F. Mohammed, E. Vauthey, J. Phys. Chem. A 112 (2008) 3823–3830.
[31] M. Maafi, L.Y. Lee, J. Pharm. Sci. 104 (2015) 3501–3509.
[32] M. Maafi, W. Maafi, Int. J. Pharm. 471 (2014) 544–552.
[33] M. Maafi, L.Y. Lee, J. Pharm. Biomed. Anal. 110 (2015) 34–41.
[34] N.J. Turro, V. Ramamurthy, W. Cherry, W. Farneth, Chem. Rev. 78 (1978) 125–145.
[35] J. Waluk (Ed.), Conformational Analysis on Molecules in Excited States, Wiley-VCH, 2000.
[36] ICH(S10), ICH Harmonised Tripartite Guideline Photosafety Evaluation of Pharmaceuticals, 2013 S10 Available at: http://www.ich.org/products/guidelines/safety/article/safety-guidelines.html (Accessed on 5 May 2016).
[37] H.J. Kuhn, S.E. Braslavsky, R. Schmidt, Pure Appl. Chem. 76 (2004) 2105–2146.
[38] ICH, Guidelines for industry Q1b photostability testing of new substances and products, Fed. Regist. 62 (1996) 27115–27122.
[39] C.A. De Azevedo Filho, D. De Filgueiras Gomes, J.P. De Melo Guedes, R.M.F. Batista, B.S. Santos, J. Pharm. Biomed. Anal. 54 (2011) 886–888.
[40] S.W. Baertschi, Drug Stab. 1 (1997) 193–195.
[41] M. Montalti, A. Credi, L. Prodi, M.T. Gandolfi, Handbook of Photochemistry, 3rd ed. CRC Press Taylor & Francis, Boca Raton, 2006.